Supporting Information for

Surface Ligand-Mediated Synthesis of Chemically Tailored Two-dimensional All-Inorganic Perovskite Nanocrystals under Ambient Conditions

Andrew H. Davis,[†] Shuya Li,[‡] Hanjie Lin,[†] Chun Chu,[†] John M. Franck,[†] Gyu Leem,[‡,§] Mathew M. Maye,[†] and Weiwei Zheng*[,†]

[†]Department of Chemistry, Syracuse University, Syracuse, New York 13244, United States
[‡]Department of Chemistry, State University of New York College of Environmental Science and Forestry, Syracuse, New York 13210, United States
[§]The Michael M. Szwarc Polymer Research Institute, Syracuse, New York 13210, United States

Corresponding Author
*wzhen104@syr.edu

Table of Contents

A. Long-ligand (18-carbon chain) control experiments. 2
   a. **Figure S1.** Optical data for long ligand composition control. 3
   b. **Figure S2.** TEM analysis for long ligand composition control. 4
B. Short-ligand (8-carbon chain) control experiments. 5
   a. **Figure S3.** Optical data for short ligand composition dependent 6
   b. **Figure S4.** AFM analysis of long ligand vs. mixed ligand synthetic composition. 7
C. Control experiments of precursor injection time. 8
   a. **Figure S5.** Optical data for injection time control. 8
   b. **Figure S6.** TEM analysis of injection time control. 9
D. Full data set of Mn-concentration dependent optical properties. 10
   a. **Figure S7.** Halide composition dependent undoped $CsPbX_3$ TEM images. 10
   b. **Figure S8**. Mn-concentration dependent optical properties of $CsPbCl_3$ NPLs. 11
   c. **Figure S9**. Mn-concentration dependent Mn:$CsPbCl_3$ TEM images. 12
   d. **Figure S10.** Mn-concentration dependent Mn:$CsPbCl_2Br$ TEM images. 12
E. References

A. Long-ligand Control Experiments

Ligand concentration and compositional control experiments initially focused on oleic acid (OA) -to- oleylamine (OAm) long-ligand composition, according to volumetric OAm concentration ([OAm]), with respect to total ligand volumetric concentration. [OAm] was varied from 0% to 100% while varying total ligand concentration between 50 and 250 μL for a 1 mL perovskite precusor. Therefore, increased [OAm] would require decreased [OA] to maintain the consistent volume. The optical spectra found in Figure S1 were analyzed for 3 distinct factors throughout all control experiments, where namely a spectra with a blue-shifted emission, narrow FWHM, and relatively high PL QY would be preferred as indicators of anisotropic growth in the resulting NCs. The resulting NCs were also analyzed using TEM (Figure S2) to ensure the use of quality NCs with high monodispersity.

Optical results, as shown in Figure S1 (a-e), indicate that the use of [OAm] of 20% - 40% are preferred as this region demonstrated spectra with blue-shifted emissions to around 509 nm, narrow FWHM as narrow as 12 nm, and PL QYs of over 30%. These results were narrowed to the use of 20% [OAm] and 80% [OA] due to these samples showing quality emission and absorption spectra, the highest PL QY, the narrowest FWHM, and relatively short PL lifetimes of the 20% to 40% [OAm] spectra with a comparable blue-shift to the other spectra.

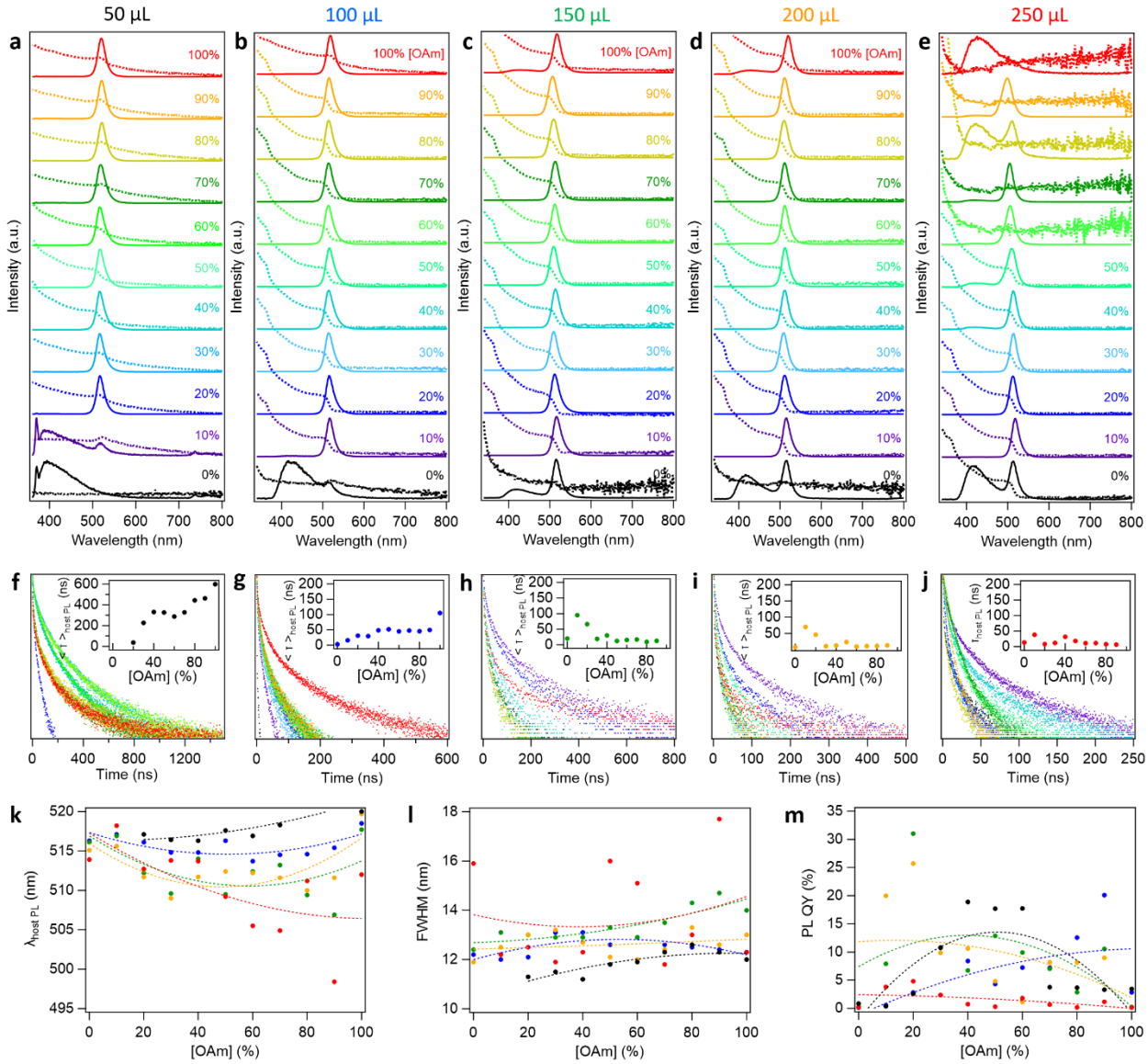

Figure S1. Long ligand compositional study of varying total volumetric concentrations from 50 to 250 µL with each volumetric concentration varying in long ligand composition form 0% OAm to 100% OAm. (a – e) Absorbance (dashed line) and photoluminescence (solid line) spectra of $CsPbBr_3$ NCs with respect to long ligand volumetric concentration from (a) 50 µL to (e) 250 µL with respect to long ligand composition of varying OA to OAm composition from 0% OAm (bottom, black) to 100% (top, red). (f – j) Time-dependent PL spectra for the varying ligand volumes and [OAm] where (f) represents the 50 µL sample and (j) represents the 250 µL sample. Insets show the average PL lifetime decay for the given samples. (k – m) Optical analysis of the given spectra for (k) host PL peak position, (l) host PL FWHM, and (m) total spectral PL QY, all with respect to [OAm].

The 20% [OAm] samples with varying total volumetric concentrations from 50 to 250 µL were analyzed using TEM (Figure S2 a – e). Each image was analyzed for both NC length (Figure S2 f – j) and surface area (Figure S2 k – o), showing ligand concentrations between 100 and 150 µL could technically be applicable for our methods, as the resulting NCs were highly monodisperse with NCs of high quality. The 100 µL NC sample exhibited avg. 19 nm in lateral length with avg. 344 nm^2 surface areas. At 150 µL, the NCs are avg. 18 nm in length with avg. surface areas ~333 nm^2. Other samples have poor NC quality and high size dispersion, where 50, 100, 150, 200, and 250 µL of ligand resulted in NCs ranging lateral lengths of 8 – 58 (avg. 18) nm , 11 – 46 (avg. 19), 12 – 26 (avg. 18) nm, 7 – 53 (avg. 19) nm, and 9 – 28 (avg. 14) nm with surface areas ranges of 64 – 2320 (avg. 348) nm^2, 163 – 895 (avg. 344) nm^2, 183 – 494 (avg. 333) nm^2, 78 – 1563 (avg. 387) nm^2, and 81 – 793 (avg. 212) nm^2, respectively. The 150 µL ligand concentration was therefore selected as it also provided a higher PL QY, narrower PL FWHM, and highly monodispersed NCs.

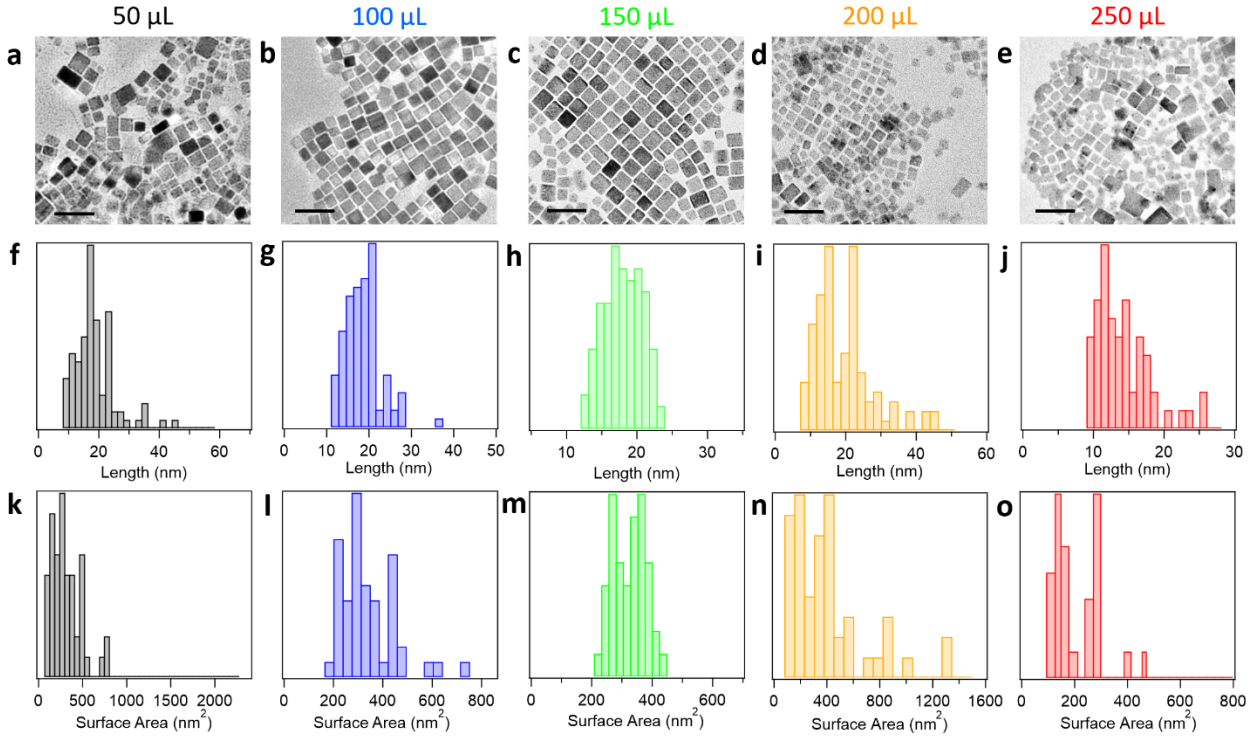

Figure S2. Long ligand compositional study based on volumetric concentration of oleic acid and oleylamine ligands at a 80% to 20% volumetric ratio from a total of 50 µL to 250 µL ligands, respectively for the synthesis of $CsPbBr_3$ NCs. TEM images (a – e) of the resulting NCs at increasing volumetric concentrations from (a) 50 µL to (e) 250 µL. Size characterization of the NCs in the given TEM images where (f) through (j) represent lengthwise measurements of the nanocube crystals and (k) through (o) represent the measured particle surface area based on the NC lateral dimensions.

B. Control Experiments of the Mixture of Short and Long Ligands

Short-ligand compositional studies were performed under a constant [long ligand] composition of 80% OA and 20% OAm. Total [short ligand] was varied from 10% to 20% and [Oct. Ac.] composition was varied from 0% to 100%, respectively (Figure S3). Low [short ligand] concentrations were originally chosen by comparison to previously reported works by Manna et al.[1] and Zheng et al.[2] which showed that low concentrations of short ligand assisted in the synthesis of anisotropic NCs. Meanwhile short ligand composition, varying from 0% to 100% [OctAc], was tested for our desired blue shift, narrow FWHM, and high PL QY for an optimized 2D NC system. Additionally, time-dependent photoluminescence was used in correspondence with our other three desired properties to further characterize our samples, in which shorter decay times are likely to resolve in anisotropic NC systems due to the increase in exciton binding energy observed with increased quantum confinement in anisotropic NCs.

These values can be narrowed by just focusing on 20% [short ligand] samples, which have the most consistent results and lowest overall lifetime. The results showed that higher [Oct. Ac.] at total 20% [short ligand] were preferred as they produced the desired narrow FWHM, blue-shifted emission, high PL QY, and short lifetime decay (Figure S3). Specifically, the region at 65% to 95% [Oct. Ac.] produced the best results, with blue-shifted emissions from 501 – 508 nm, FWHM from 12 – 16 nm, PL QY up to ~40%, and relatively short average lifetime decays that averaged around 50 ns. We see that the appropriate range for [Oct. Ac.] shifts to between 60% and 80%, resulted in similar PL peak positions, FWHM, and PL QY as the other [short ligand] samples, showing blue shifted emissions to 503 nm, FWHM down to ~12 nm, and PL QY up to ~40% with little variance based on [short ligand]. Thus the [Oct. Ac.] was chosen to be 75% due to its decreased lifetime, increased PL QY, and relatively similar, blue-shifted PL and PL FWHM. Selected ligand conditions, therefore, involve the use of a total 150 µL ligands, consisting of 80% long ligands (96 µL (64%) OA and 24 µL (16%) OAm) and 20% short ligand (22.5 µL (15%) OctAc, and 7.5 µL (5%) OctAm), at a total volumetric concentration of 150 µL for a 1 mL precursor solution. Results from $CsPbBr_3$ studies were also shown to translate to $CsPbCl_3$ and mixed halide NCs with a substantial narrowing of the emission FWHM resulting with increasing [Cl^-] anion concentration.

Results showed a preference for higher concentrations of OctAc for characteristics consistent with 2D growth, including blue shifted PL, thinner FWHM, and shorter PL lifetime decay, where peak position consistently blue shifted for all samples up to ~90% [OctAc], FWHM consistently decreased with [OctAc] up to 100%, PL QY peaked at an average of ~30% at ~80% [Oct Am] and PL lifetime decay duration decreased with [OctAc] up to 100%. While PL peak position, PL FWHM, and PL QY depended more heavily on ligand composition than concentration, the average time-dependent PL decay depended much more significantly on [short ligand], where higher concentrations consistently resulted in shorted average decay times.

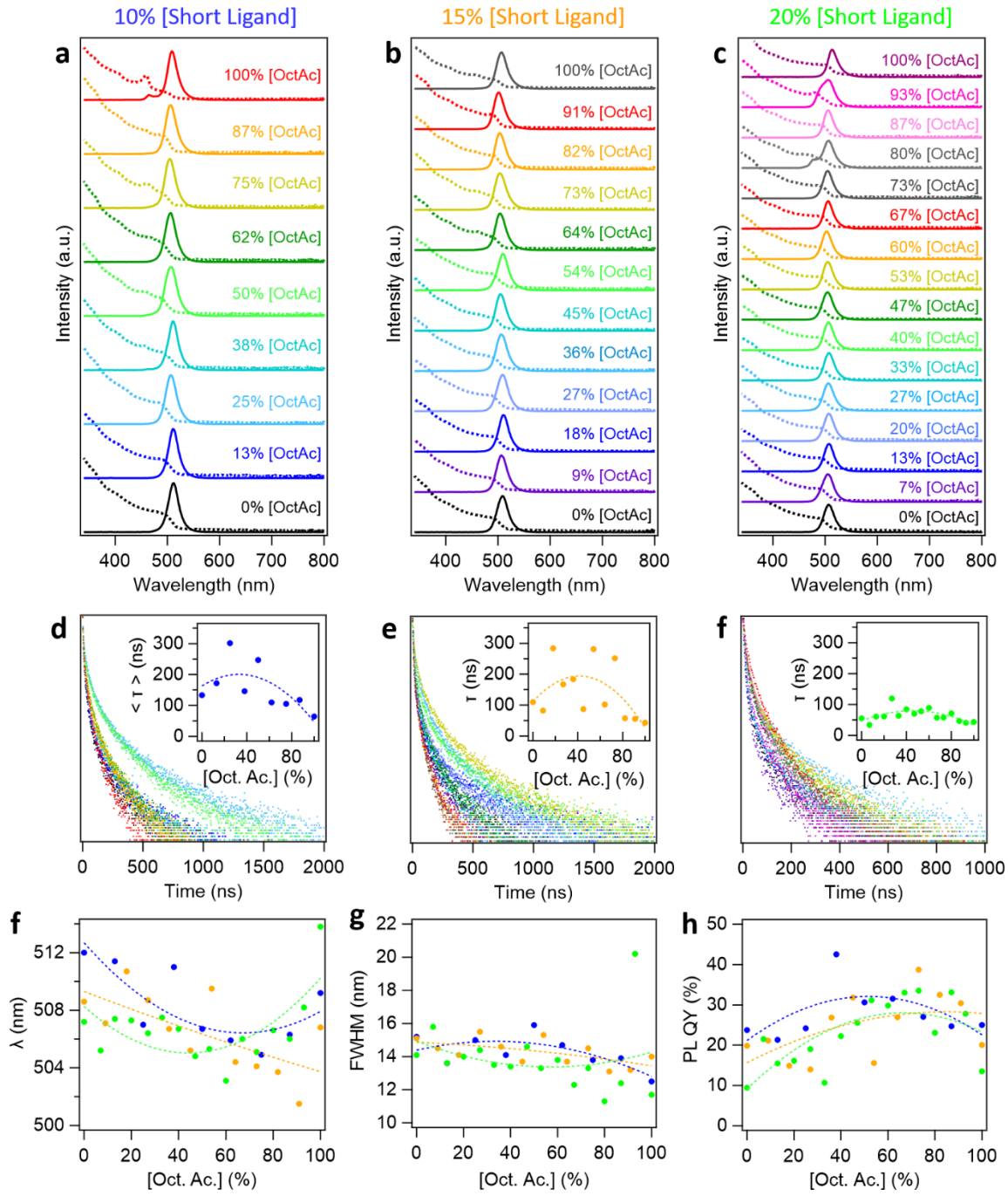

Figure S3. Short ligand compositional study at a consistent 80% oleic acid to 20% oleylamine long ligand composition where the ratio between short ligands (v:v) was tested at the desired 10 – 20% short ligand concentration range with respect to [OctAc] form 0 – 100%. (a-c) Absorption (dashed line) and PL (solid line) spectra for (a) 10%, (b) 15%, and (c) 20% [total short ligand]. (d-f) Time-dependent PL spectroscopy was obtained for (d) 10%, (e) 15%, and (f) 20% [total short ligand] with respect to [OctAc]. The average calculated lifetime decay for these samples is displayed in inset. Represents the optical analysis of these spectra for (f) PL peak position, (g) PL FWHM, and (h) PL QY, where ligand concentrations (10%, 15%, 20%) were compared.

AFM was used to determine and analyze the height of two representative $CsPbBr_3$ samples. One $CsPbBr_3$ sample was synthesized using the optimized long ligand composition of 80% OA to 20% OAm at a total volumetric ligand concentration of 150 µL. The other sample was synthesized using the optimized long and short ligand mixture of 64% OA, 16% OAm, 15% OctAc, and 5% OctAm at a total volumetric ligand concentration of 150 µL. When comparing the height data of the long-ligand only sample (Figure S4a – S4c) to the TEM data for the same sample above (Figure S2c and S2h), we can compare the lateral (18 nm) and vertical (7.4 nm, ~12 monolayer (ML)) growth of these NCs. This indicates that resulting NCs are either quasi-nanoplatelets (QNPLs) or NPLs. Although, 12 MLs in thickness is typically larger than traditional NPL, therefore we will refer to these NCs as QNPLs. Meanwhile, the AFM of our short ligand containing system in Figure S4d to S4f resulted in NCs of ~4.8 nm thickness, showing that short ligand introduction caused thinner NC formation toward more accurately interpretable NPLs.

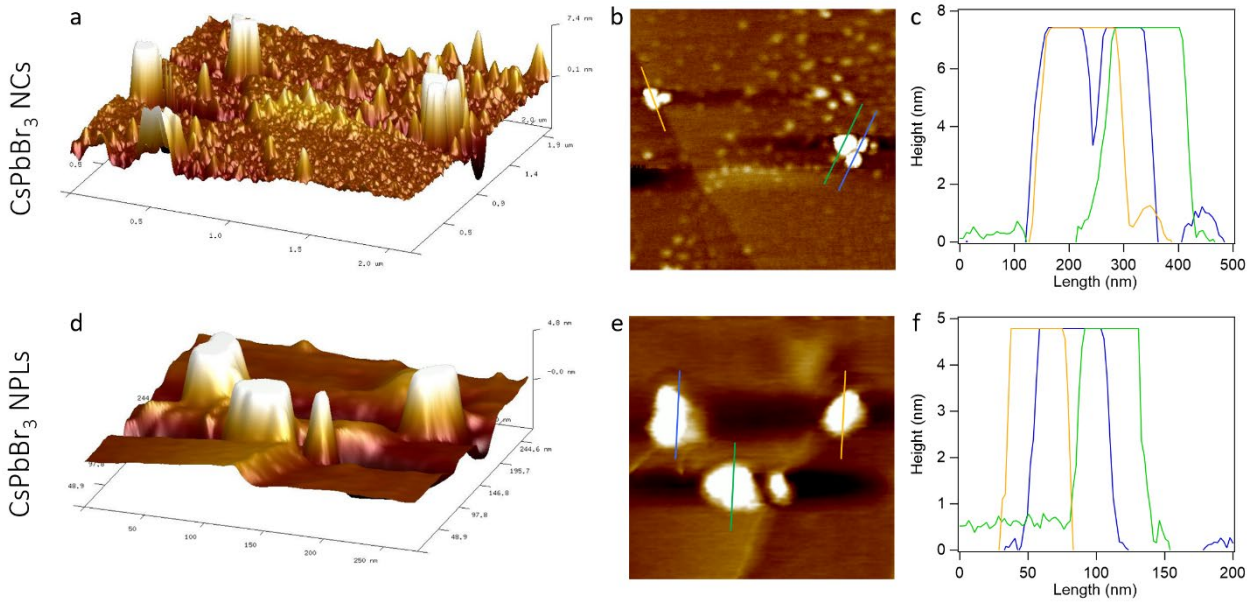

Figure S4. AFM image comparison for $CsPbBr_3$ QNPLs, synthesized using the optimized long ligand concentration and composition of 80% OA to 20% OAm at 150 µL total volumetric concentration and 2D $CsPbBr_3$ NPLs, synthesized using the standard 62% OA, 16% OAm, 15% OctAc, and 5% OctAm mixture of long and short ligands at 150 µL total volumetric concentration. (a, d) 3D tapping phase topographical image of $CsPbBr_3$ (a) QNPLs and (d) NPLs. (b, d) 2D tapping phase topographical image of $CsPbBr_3$ (b) QNPLs and (e) NPLs. (c, f) Cross-sectional height analysis of a representative particles for $CsPbBr_3$ (c) QNPLs and (f) NPLs.

C. Control experiments of precursor injection time

Injection time was determined to be an important parameter for our reactions, largely controlling the quality of the resulting product. Rapid, near instantaneous, injection times resulted in poor NC quality control as shown in Figure S5 and S6. Generally, multiple emission spectra and poor-quality absorption spectra resulted from rapid injections. NC quality increased with injection times but mostly plateaued after 60 sec of dropwise injection.

By slowing the reaction, NC solutions with high monodispersity and high overall quality were produced. This is likely because toluene enacts the NC reaction by forcing rapid nucleation. Therefore, slowing the injection time allows for NC growth, rendering 2D NPLs formation. The effects of injection time on NC formation can be observed in Figure S5, where the instantaneous injection NPL for CsPbBr3 (Figure S5a) shows a broad PL with a poor quality absorption spectra and the $CsPbCl_3$ reaction is polluted with multiple emission spectra, both indicating poor monodispersity. While long injection time (> 60 s) generally leads to broader size distribution as indicated by broader FWHM, increasing from ~15 to 18 nm between 60 and 180 sec for $CsPbBr_3$.

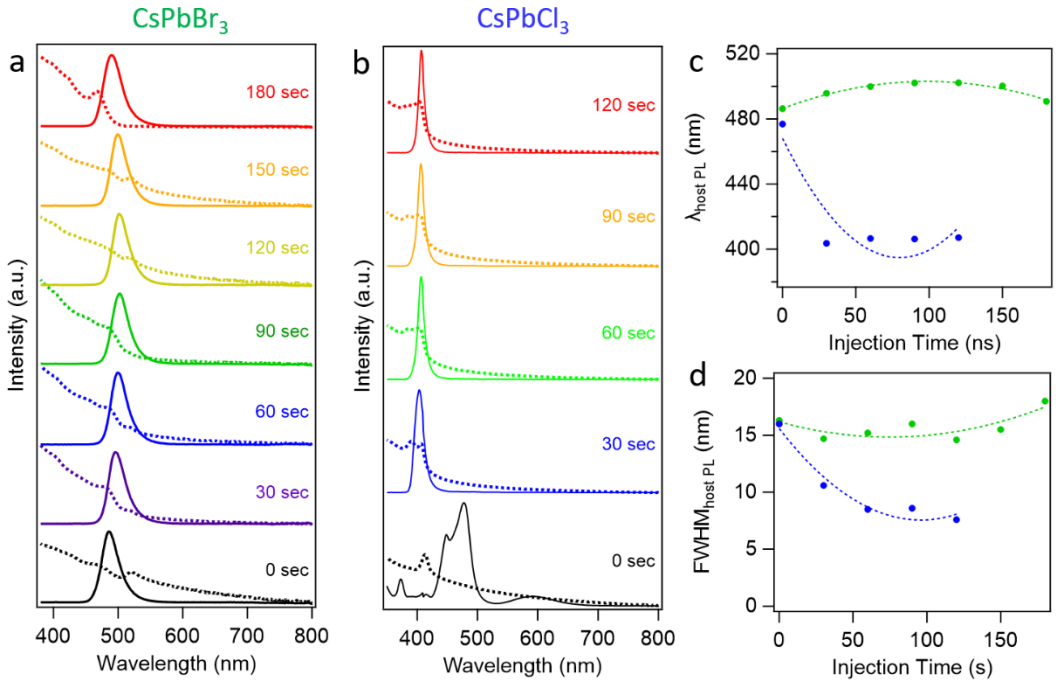

Figure S5. Injection time and solvent dependent Absorption (dashed line) and PL (solid line) of (a) $CsPbBr_3$ and (b) $CsPbCl_3$ NCs from 0 sec to up to 180 sec (c) PL peak position and (d) PL FWHM of samples made using the optimized long-ligand only system.

To further elucidate the NC quality with respect to injection time, TEM images were obtained for $CsPbCl_3$ NCs with varying injection time from 0 to 60 seconds. The resulting TEM images, show that rapid injection times result in a NC solution contains dark clouded regions consisting of small quantum dot side-products. Longer injection times result in less quantum dots, and eventually no observable small dots in the 60 second injection sample. Therefore, 60 sec injection times were chosen for our reaction conditions as it provided high quality nanocrystals without limiting or overly lengthening the reaction process.

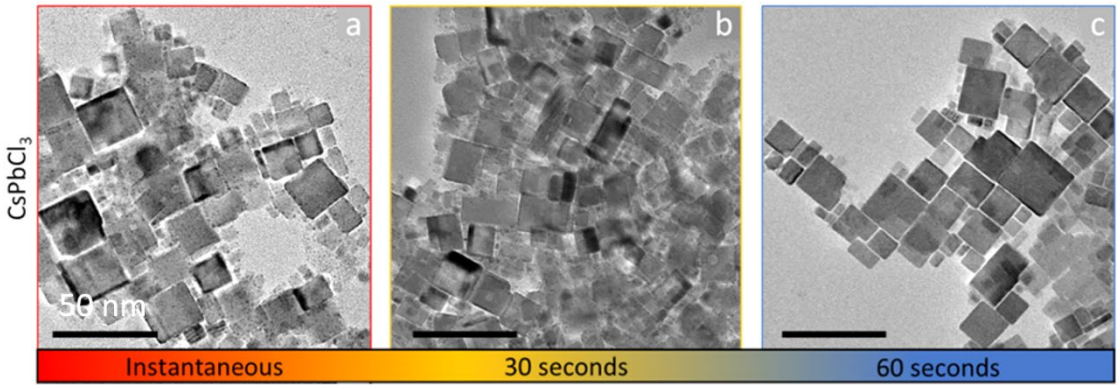

Figure S6. Injection time dependent TEM images of (a – c) $CsPbCl_3$ NPLs, where the Cs-Pb NC precursor injections into toluene were performed (a) rapidly, (b) over 30 s, and (c) over 60 s injection times.

D. Full data sets of the representative data depicted in the main manuscript

Undoped $CsPbX_3$ NPLs were synthesized as a direct comparison to the later depicted Mn:$CsPbX_3$ samples. TEM images, given in Figure S7, show that the variance of the X-site halide does not largely change the dimensions or shape of the resulting NPL samples.

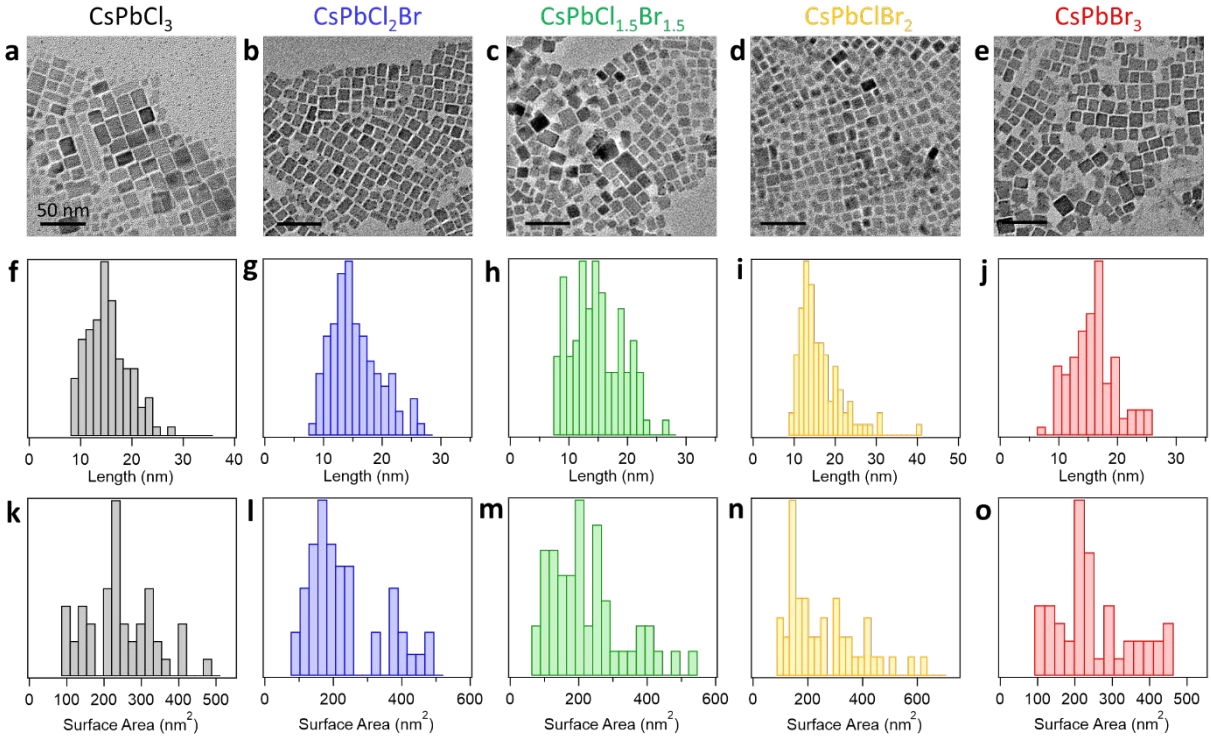

Figure S7. TEM images of undoped (a) $CsPbCl_3$, (b) $CsPbCl_2Br$, (c) $CsPbCl_{1.5}Br_{1.5}$, (d) $CsPbClBr_2$, and $CsPbBr_3$ NPLs with respective (f – j) NPL lateral size and (k – o) surface area measurements.

Mn doping in 2D $CsPbCl_3$ NPLs was attempted over a wide range of Mn dopant molar concentrations, from 25 – 400% Mn:Pb %mol in synthesis. Generally, larger doping concentrations, in these samples, result in a more reds-shifted dopant emission, a higher dopant-to-host intensity ratio, and a short host and Mn lifetime. The PL QY increases from 0-200% [Mn] in synthesis then decreases with higher [Mn] due to Mn dopant concentration quenching effect. In the full data set, these trends are clear, however, multiple points were removed from the data presented in Figure 2 in the main manuscript since the data trend can be maintained with less points making the data more evident and concise in the main manuscript.

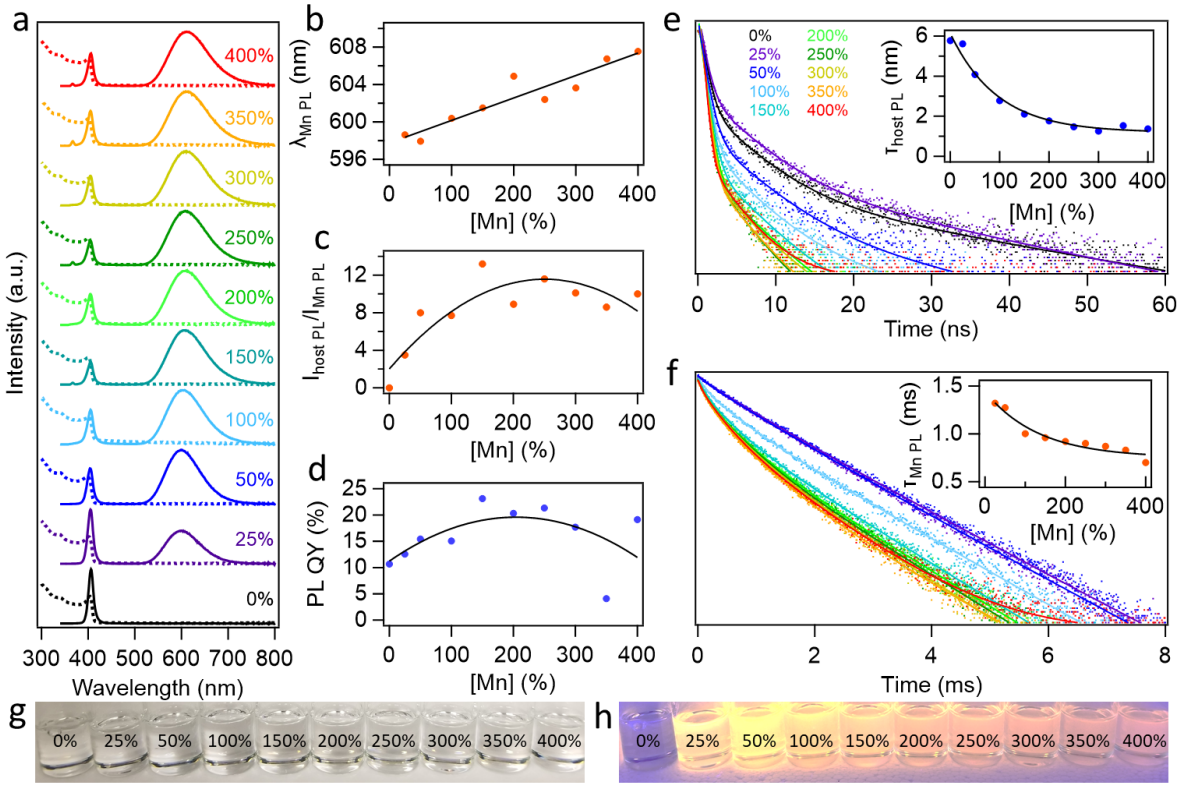

Figure S8. Mn concentration dependent optical properties of doped $CsPbCl_3$ NPLs from 0% to 400% [Mn] in synthesis. (a) Absorption (dashed lines) and PL (solid lines) spectra with corresponding (b – d) spectral analysis by (b) Mn PL peak position, (c) Mn-to-host PL integrated peak area ratio, and (d) total spectral PL QY. Time dependent PL for (e) Host PL and (f) Mn PL (inset: average PL lifetime Decay for the given samples with respect to [Mn]). (g – h) Images of 2D Mn:$CsPbCl_3$ NPLs in toluene solution under (g) visible light and (h) 365 nm UV-light irradiation.

Similar to the optical data in Figure S8, select TEM images for Mn:$CsPbCl_3$ NPLs were selected for the main manuscript to mitigate cluttering and present the data in an approachable manner. Therefore, the TEM images for Mn:$CsPbCl_3$ varying in Mn-dopant concentration form 0.2% to 1.3% Mn are provided below in Figure S9. These resulting NPLs measure an average of approximately 17, 19, 18, and 19 nm from 0.2% to 1.3% [Mn], respectively, demonstrating consistent morphology independent of dopant concentration.

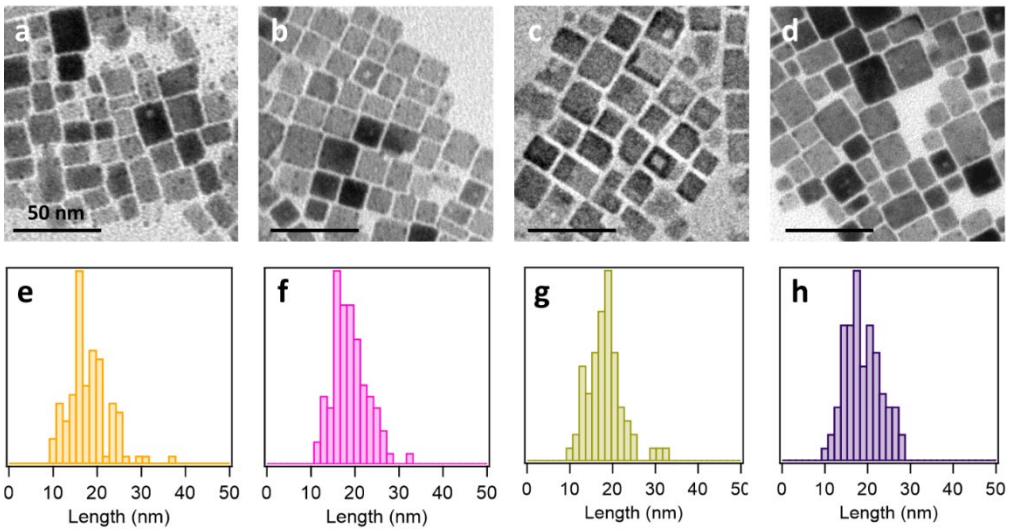

Figure S9. TEM images of (a) 0.2%, (b) 0.5%, (c) 0.9%, and (d) 1.3% Mn-doped $CsPbCl_3$ NPLs with (e – h) respective lateral size analysis.

Additionally, Mn:$CsPbCl_2Br$ NPLs were synthesized with varying Mn-dopant concentrations from 0.2% to 1.2% mol% of Mn to represent mixed halide NPLs with varying [Mn]. The resulting NPLs measured an average of approximately 16, 18, 17, and 18 nm lateral size, with respect to increasing dopant concentration.

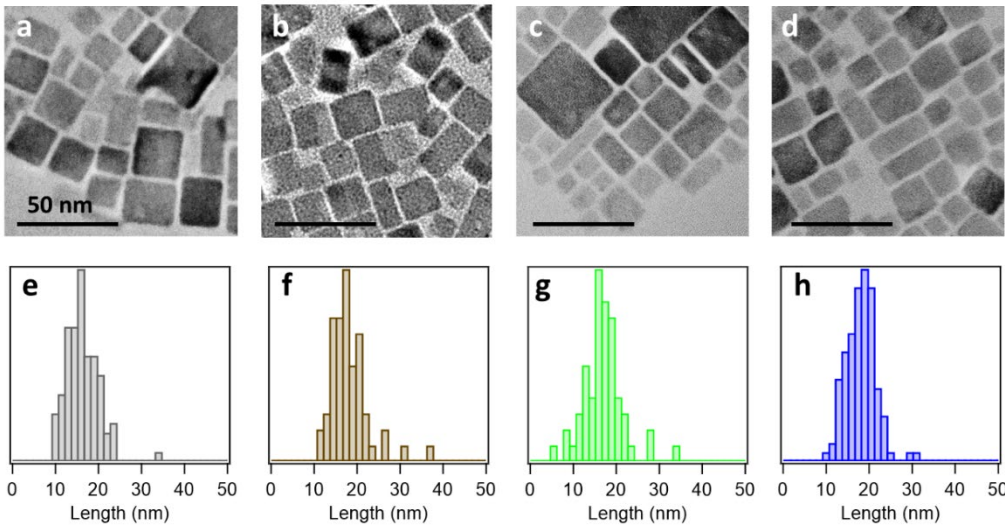

Figure S10. TEM images of (a) 0.2%, (b) 0.5%, (c) 0.8%, and (d) 1.2% molar Mn-dopant introduction $CsPbCl_2Br$ NPLs with (e – h) respective lateral size analysis.

References.

(1) Shamsi, J.; Dang, Z.; Bianchini, P.; Canale, C.; Stasio, F. D.; Brescia, R.; Prato, M.; Manna, L., Colloidal Synthesis of Quantum Confined Single Crystal $CsPbBr_3$ Nanosheets with Lateral Size Control up to the Micrometer Range. *J. Am. Chem. Soc.* **2016,** *138,* 23, 7240-7243.

(2) Li, Z.-J.; Hofman, E.; Davis, A. H.; Maye, M. M.; Zheng, W., General Strategy for the Growth of $CsPbX_3$ (X = Cl, Br, I) Perovskite Nanosheets from the Assembly of Nanorods. *Chem. Mater.* **2018,** *30,* 11, 3854-3860.